SCIENTIFIC REPORTS

OPEN

SUBJECT AREAS:
POROUS MATERIALS
SOLAR CELLS

Received
3 June 2014

Accepted
17 September 2014

Published
13 October 2014

Correspondence and requests for materials should be addressed to L.W. (lothar.wondraczek@uni-jena.de)

Optical breathing of nano-porous antireflective coatings through adsorption and desorption of water

Karsten H. Nielsen[1], Thomas Kittel[1], Katrin Wondraczek[2] & Lothar Wondraczek[1]

[1]Otto Schott Institute of Materials Research, University of Jena, Fraunhofer Str. 6, 07743 Jena, Germany, [2]Leibniz Institute of Photonic Technology e.V., Albert-Einstein-Str. 9, 07745 Jena, Germany.

We report on the direct consequences of reversible water adsorption on the optical performance of silica-based nanoporous antireflective (AR) coatings as they are applied on glass in photovoltaic and solar thermal energy conversion systems. In situ UV-VIS transmission spectroscopy and path length measurements through high-resolution interferometric microscopy were conducted on model films during exposure to different levels of humidity and temperature. We show that water adsorption in the pores of the film results in a notable increase of the effective refractive index of the coating. As a consequence, the AR effect is strongly reduced. The temperature regime in which the major part of the water can be driven-out rapidly lies in the range of 55°C and 135°C. Such thermal desorption was found to increase the overall transmission of a coated glass by ~ 1%-point. As the activation energy of isothermal desorption, we find a value of about 18 kJ/mol. Within the experimental range of our data, the sorption and desorption process is fully reversible, resulting in optical breathing of the film. Nanoporous AR films with closed pore structure or high hydrophobicity may be of advantage for maintaining AR performance under air exposure.

Antireflective (AR) coatings are widely applied to optical components in order to improve optical transmission at material surfaces or interfaces, e.g., on cover glasses of photovoltaic modules or solar thermal energy conversion systems, lenses, windows and various other devices[1,2]. The AR effect usually relies on destructive interference of light which is reflected from the immediate surface and the interface between surface and coating[3]. Consequently, AR coatings are designed according to Fresnel's law where optimal antireflection is obtained for layers with a thickness of $\lambda/4$ and a linear refractive index corresponding to the square root of that of the substrate. For glasses which are employed in architecture, solar modules and automotion, the optimal index of the coating is in the area of 1.23–1.27. Such low refractive indices cannot readily be obtained in a bulk material. Instead, an effective medium consisting of high-index particles and low-index pores can be created[4]. Technologically, this is usually achieved on large area through deposition of a nano-porous layer of silica where the pores are filled with a low-index medium (air).

However, depending on relative humidity, pores in SiO_2-based materials tend to readily adsorb water[3] from the surrounding atmosphere, and also organic compounds[5,6] or carbonates[7]. Such contamination may have significant implications for the remaining AR effect or even spoil it by inducing an increase of the effective refractive index of the coating. This is schematically illustrated in Figure 1 for a coating in which the pores are filled with water, Fig. 1(a) vs. air, Fig. 1(b). In addition to the optical effect, the presence of water in the coating can also provoke corrosion and facilitate further soiling of the surface[8]. In this context hydrophobic AR coatings have been shown to be more robust towards humid corrosion[1] and less prone to water adsorption in the pores[9].

The dynamic uptake and release of water, the so-called breathing, of a TEOS derived AR coating has been investigated by infrared spectroscopy by Vong and Sermon[3]. Other techniques such as the use of a quartz crystal microbalance[10] or environmental ellipsometry, were also employed by other groups to characterize the water adsorption on sol-gel (tetra ethyl orthosilicate, TEOS) based systems, coated on silicon[6] and on polymer substrates[9]. It was demonstrated that in such coatings, water is reversibly adsorbed in the pores both physically and chemically. Formation of silanol groups takes place at room temperature[3,6], but for condensation it requires higher temperature (~190°C)[11]. For highly-ordered mesoporous silica films, molecular adsorption and capillary condensation could be distinguished from X-ray reflectivity measurements[12]. The water uptake by such coatings was shown to increase the overall thickness of the coating by swelling (of the pores) and by condensation of a water film on the rough surface of the coating. Further, the swelling of porous sol-gel based coatings induces pore

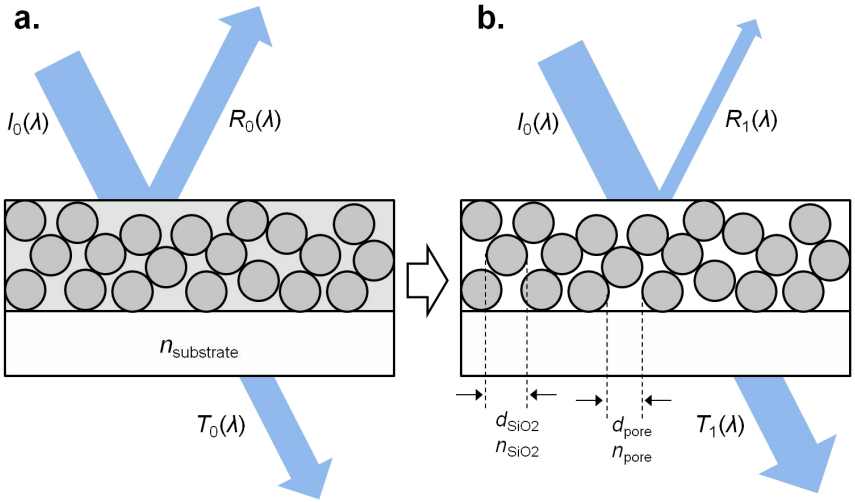

Figure 1 | Schematic illustration of the effect of water adsorption on the transmission of a glass substrate coated with a nano-porous antireflective silica coating. When the pores are filled with water (case a), the effective index of the coating results from the mixture of water and silica according to the volume fraction of each component. For air-filled pores (case b), the index reduces notably, leading to significantly lower reflectivity.

deformations that alter the mechanical properties[10]. Noteworthy, also the structure of the water molecules in such nanometric confinement is of interest in many branches of science (e.g. ref. 13).

While the previous studies investigated the mechanisms and long-term behavior of environmental ageing effect under mostly isothermal conditions for different coatings, in this this paper, we propose a simple and direct method to analyze the effects of water adsorption and desorption on the optical performance of AR coatings. For that, adsorption-desorption cycles were performed at varying temperature between 30°C and 75°C and observed in situ by interference microscopy and transmission spectroscopy. The significantly improved accuracy of the interferometric data aquisition as compared to ellipsometry enables quantification of even slight variations in coating properties without the need for further mathematical models and assumptions for data treatment.

Results

Characterization of the as-prepared films. The thickness of the as-obtained coating was determined as (120 ± 20) nm. The AR effect is validated by comparing the transmission spectra of non-coated and coated glass substrate as shown in Fig. 2. The transmission maximum is obtained near 520 nm which correlates well with the film thickness which is supposed to be $\lambda/4$ for the wavelength of maximum transmission[4]. The transmission enhancement at this wavelength is by about 3.3 percent points, i.e., from ~ 91.4% (uncoated, optical absorption ~ 0.6%/mm at this wavelength) to 94.7% (coated) for a double-sided coating.

Assuming a substrate refractive index of 1.52 (corresponding to a reflectivity of ~ 4% of an uncoated glass surface), the observed increase corresponds to a refractive index of the coating of 1.438, applying Eq. 1[4], where R is reflectivity from a single side, and n_c, nsubstrate and n_{air} are the refractive indices of the coating, the glass substrate and the surrounding medium respectively.

$$R = \left(\frac{n_c^2 - n_{substrate} n_{air}}{n_c^2 + n_{substrate} n_{air}} \right)^2 \qquad (1)$$

This calculated value is somewhat lower than the value which was estimated by ellipsometry.

Effect of humidity on overall transmission. The effect of loading an uncoated and coated sample under the same humid conditions on the absorbance spectra in the infrared range is also illustrated in Fig. 2. As expected, the coated sample adsorbs more water than the uncoated reference sample as it is indicated by pronounced absorbance intensities at the characteristic wavelengths of OH stretching vibrations in the spectral range around 3000 cm^{-1} to 3500 cm^{-1}. That is, the transmission increase which is caused by the coating is significantly lower at the characteristic absorption bands relative to the overall increase which is predicted by the simple consideration of interference. In detail, the peaks at 3230 cm^{-1} and 3400 cm^{-1} can be assigned to stretching vibrations of –OH from two types of absorbed water[14], that is, solid-like and liquid-like, respectively. The band at 3650 cm^{-1} is attributed to Si-OH stretching vibrations[3]. The elevated absorbance values in this wavenumber region indicate that the coated samples adsorb water both chemically and physically. The less pronounced but visible absorbance peaks at around 2849 cm^{-1} and 2915 cm^{-1} are assigned to -CH_2 stretching vibrations[15], and are attributed to atmospheric contaminants.

Effect of temperature on overall transmission. Further evidence for the fact that water adsorption is responsible for the observed deviations is provided by thermal desorption experiments. These were conducted as follows, starting with samples which were kept at laboratory conditions before measurements. First, the humidity

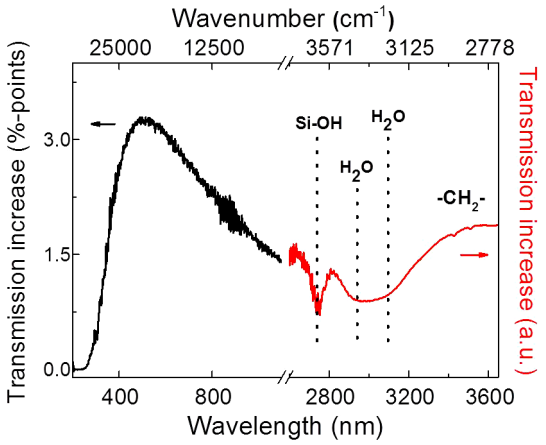

Figure 2 | Transmission difference spectra between an as-received double-side coated and an uncoated glass for the UV-VIS and infrared spectral ranges. The peak assignments are explained in the text below in the next sub-chapter.

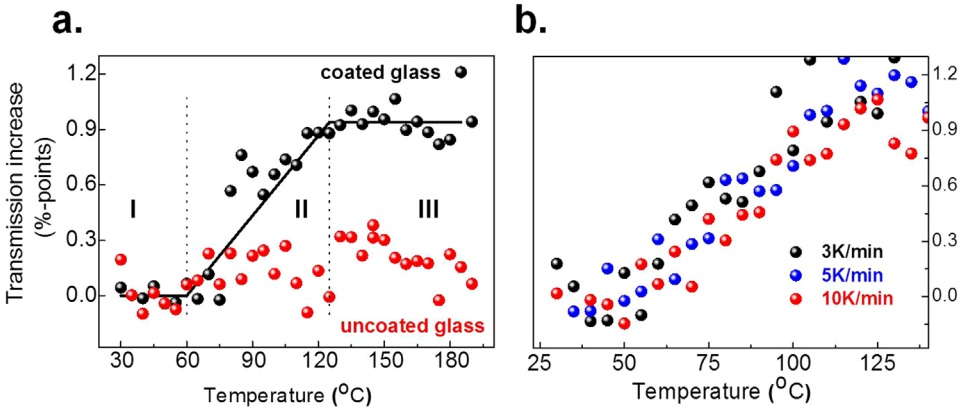

Figure 3 | (a) Relative change in transmission as a function of temperature for coated glass and uncoated glass at a wavelength of 520 nm and for the heating rate of 5 K/min. The lines are guides to the eye. The desorption regions I-III as described in the text are indicated with dashed lines. In (b), the heating rate dependency of the desorption-induced increase in transmission is shown for region II.

conditions were kept constant while changing the sample temperature. The relative change of transmission at 520 nm as a function of temperature is displayed in Fig. 3(a). In case of the bare glass sample, the transmission remains more or less at the same level. In case of the AR-coated glass, the transmission experiences a change with temperature. For the coated glass, an overall increase of the relative transmission of ~ 1%-point is observed in the studied temperature range. Hence, the overall transmission of the dry coated sample is ~ 1%-point higher than the previously measured 94.7%. With Eq. 1, this yields an effective refractive index of the dry coating of 1.414. From this, the porosity of the coating can be estimated according to Eq. 2, assuming that the refractive index of the pore medium is unity (air), and the effective index of the coating results from a mixture of the indices of pores and silica ($n_{SiO2} = 1.460$) according to effective medium theory[4],

$$\left(\frac{n_c^2-1}{n_{SiO2}^2-1}\right)=1-\frac{P}{100} \qquad (2)$$

A value of ~ 11.7% is obtained in this way. However, the real porosity may still be higher, as higher temperatures are needed to drive-out the last (chemisorbed) water from porous SiO_2 materials[11].

On the graph in Fig. 3(a), three regimes of iso-humid desorption can be distinguished: In the onset region I the relative transmission remains unchanged, in region II, due to water desorption, transmission increases approximately linear with increasing temperature, and finally in region III, a constant level of high transmission is reached. The three regimes can be correlated according to the process of isothermal sorption[10]: Region I corresponds to high humidity conditions where all capillaries are filled, region II corresponds to the onset of capillary evaporation, and region III corresponds to low humidity conditions. Hence, the depleted water content in the coating in region III causes a higher air-filling fraction and thus in turn a lower effective refractive index. A suggested temperature interval for the transition (60–125°C) has been marked on Fig. 3(a).

This type of experiment was repeated at heating rates of 3 K/min, 5 K/min and 10 K/min as shown in Fig. 3(b). For each of those, the same tendency of increasing transmission over the studied temperature range was observed. In particular, region II always occurs in the range of 50°C to 125°C regardless of heating rate within the range of data. We therefore conclude that in all three sets of data, the equilibrium of condensation-evaporation is reached at any point within the timescale of heating. Therefore, the observed process reflects the thermodynamics of the sorption-desorption process.

Effect of temperature on optical-path length under iso-humid conditions. The change of optical pathway is another suitable parameter to track the AR efficiency of the coated sample under iso-humid conditions. Interferometric experiments were therefore conducted in argon and air atmosphere. The normalized optical path length monitored as a function of temperature is shown in Fig. 4. Regardless of the atmosphere, there is a decrease of the normalized optical path length with increasing temperature. On the figure, a transition regime similar to the one which is observed in Fig. 3(a) is also marked (55°C–135°C). As a result of thermally-induced desorption, the coating responds with an overall decrease of ~11% (air) and of more than 25% (argon), respectively, in optical pathlength. This reflects the decrease in effective refractive index with water evaporation. The strong deviation which is seen between the data at 200°C is ascribed to chemical modifications of the silica layer taking place at higher temperature.

Upon cooling, the difference between (humid) air and argon (dry, Ar) atmosphere becomes visible: for the sample cooled in air, the optical path length returns to the point at which the prior heating scan was started. This reflects the re-increase of the effective refractive index back to its original value upon re-adsorption (of water). In dry Ar atmosphere, on the other hand, the optical path length of the coating remains unaffected by cooling as there is no water available to re-adsorb into the pores. This also indicates that the effect of thermal expansion on optical path length can be neglected.

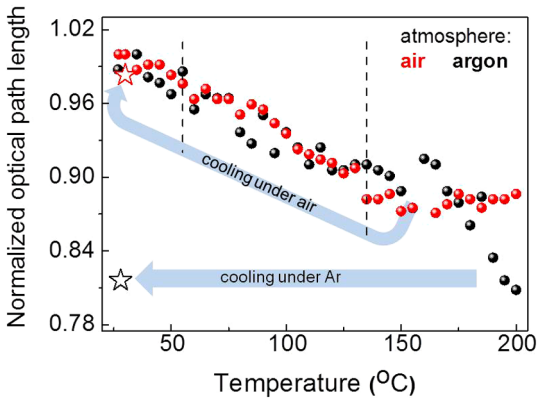

Figure 4 | **Normalized optical path length recorded as a function of temperature in two different atmospheres: Ar (5 K/min) and air (3 K/min).** Stars represent measurements after subsequent cooling. The vertical dashed lines mark the approximate position of the transition regime (corresponding to regime II in Fig. 3a) between 55°C and 135°C.

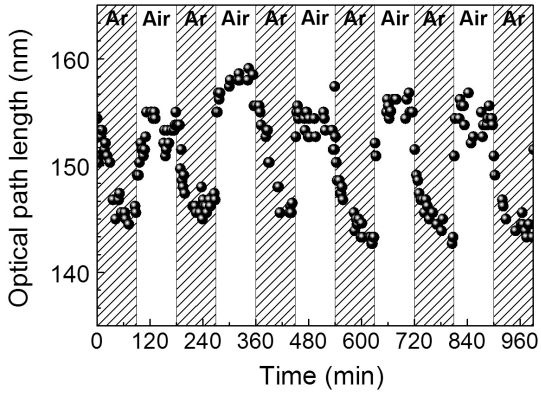

Figure 5 | Optical path length of the coating measured at constant temperature (30°C), but with changing atmosphere every 90 min between humid air and argon. The error of the pathlength measurement is ±1 nm.

Effect of optical breathing on AR efficiency. The effect of optical breathing, i.e., the reversibility of the optical path length and, hence, AR efficiency with adsorption and desorption was examined under isothermal conditions for cycling between humidified air and inert argon. This is exemplarily shown in Fig. 5. It can be seen, that the effect of water adsorption is closely following the change in atmosphere. Desorption on the other side, requires somewhat more time. The five consecutive scans which are shown in Fig. 5 are normalized and re-plotted in Fig. 6(a). In a first consideration, we conclude that the process of adsorption and desorption is fully reversible, at least for the considered number of scans. That is, there are no obvious degradation reactions occurring which would lead to permanent changes on the coating. When evaluated individually, each cycle has a very similar shape, resulting in an end level of 4–8% lower than the maximum level attained under humid atmosphere, roughly corresponding with the observed decrease upon thermal desorption as shown in Fig. 4.

Determination of average pore size. The effective (average) pore size of the water-saturated coating can be estimated with the *Kelvin* formula, Eq. 3[16–18] for the samples loaded at 80% r.h.,

$$r = \frac{-2\gamma \times \cos(\Theta)}{RT \times \ln\frac{P}{P_0}} \tag{3}$$

Here, γ and V_m are the surface tension and molar volume of water, respectively, and θ represents the wetting angle between the porous SiO_2 material and water, which is around 27°[6]. At an 80% relative humidity as present here, this corresponds to the filling of pores of radius $r \sim 4$ nm and below.

Determination of activation energy of desorption. In order to evaluate the activation energy of water desorption in the present situation, breathing experiments were conducted at several different temperatures. The kinetics of the desorption process were evaluated for the reaction coordinate ζ, (Eq.4) defined on the basis of the fractional water content of the coating, f_{H20}. The data were fitted in terms of a simple *Avrami* equation, Eq. 5[19].

$$\xi = \frac{f_{H2O} - f_{H2O\infty}}{f_{H2Oi} - f_{H2O\infty}} \tag{4}$$

$$\xi(t) = \exp\left(\frac{-t}{\tau}\right)^n \tag{5}$$

In Eqs. 4–5, f_{H2O}, f_{H2Oi}, and $f_{H2O\infty}$ represent the coating fraction of water at the actual measurement point, initially and at the end of the experiment (extrapolated to infinite time), respectively. In Eq. 5, τ is the characteristic timescale and n represents the reaction order.

Applying linear mixing for the refractive index of the coating and under the assumption of constant coating thickness and SiO_2 volume fraction during the desorption process, it can be shown that the optical path length can be inserted directly in the formula for the reaction coordinate, Eq. 6 and Eq. 7.

$$\begin{aligned} n &= f_{SiO2}\cdot n_{SiO2} + f_{air}\cdot n_{air} + f_{H2O}\cdot n_{H2O} \\ &= f_{SiO2}\cdot(n_{SiO2} - n_{air}) + f_{H2O}\cdot(n_{H2O} - n_{air}) + n_{air} \end{aligned} \tag{6}$$

$$\frac{\Delta n - \Delta n_\infty}{\Delta n_i - \Delta n_\infty} = \frac{c\cdot n - c\cdot n_\infty}{c\cdot n_i - c\cdot n_\infty} = \frac{f_{H2O} - f_{H2O\infty}}{f_{H2Oi} - f_{H2O\infty}} = \xi \tag{7}$$

An example for a fit of the data obtained at 50°C to Eq. 7 is given in Fig. 6(b). All fits gave values for the reaction order n in the range of

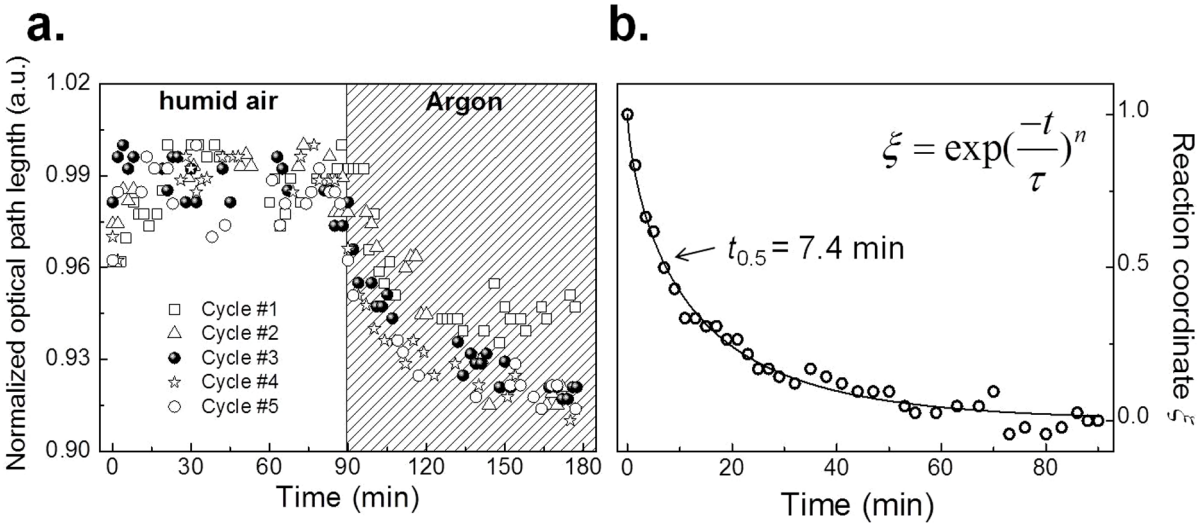

Figure 6 | (a) Normalized optical path lengh for the invidiual cycles presented in Fig 5. The optical pathlength has been normalized to the maximum value for the corresponding cycle. (b) Reaction coordinate for examplary water desorption experiment conducted at 50°C fitted to the *Avrami* equation. The time for 50% desorption $t_{0.5}$, has been marked on the graph.

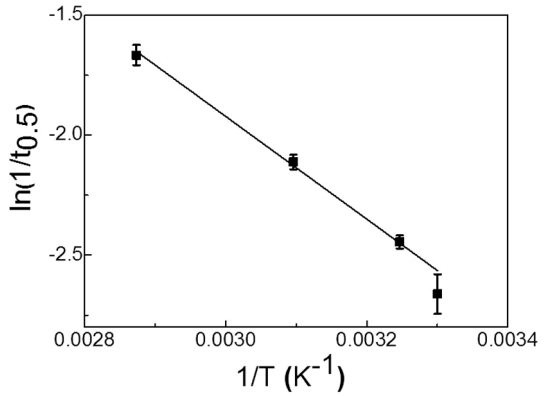

Figure 7 | *Arrhenius* plot of the drying time, $t_{0.5}$, obtained by fitting the data to an *Avrami* equation. The line represents the best fit. From the slope, the activation energy is estimated to be 18 ± 1 kJ/mol.

0.54–0.74. That is, desorption process follows a stretched exponential decay. On the other hand, water desorption from silica surfaces was previously described as a first order reaction[11,20].

For estimation of the activiation energy, the time at 50% water release, $t_{0.5}$, was determined. It was found to decrease from 14.3 min to 5.3 min with increasing desorption temperature. The values were plotted against the reciprocal temperature as shown in Fig. 7. A linear fit with a correlation coefficient of 0.98 was obtained with a slope of 2100 K^{-1} ± 121 K^{-1} corresponding to an activation energy of (18 ± 1) kJ/mol for the water desorption process. This value is somewhat lower than the 26.16 kJ/mol which have been reported for water desorption from bulk mesoporous SiO_2 (10 nm pore diameter)[21], and is also lower than the 46–49 kJ/mol which were reported for silica gels[20].

Discussion

In summary, we have studied the direct consequences of water adsorption and desorption on the optical performance of silica-based nanoporous AR coatings on glass as they are applied in photovoltaic and solarthermal energy conversion systems. Water adsorption in the pores of the film even at intermediate humidity results in a noticable increase of the effective refractive index of the coating. As a consequence, the AR effect is strongly reduced. Desorption follows three regimes which can be directly related to the three known regimes under isothermal conditions. The temperature regime in which the major part of the water can be driven-out rapidly lies in the temperature range of 55°C and 135°C. We also report activation energy and desorption timescale in isothermal conditions, which can be used to judge technical applications. Within the experimental range of our data, the sorption and desorption process is fully reversible, resulting in "*optical breathing*" of the film. Secondary effects such as the promotion of substrate corrosion through accumulation of water in the film, however, cannot be excluded. Nanoporous AR films with closed pore structure or high hydrophobicity may be of advantage for maintaining AR performance under air exposure.

Methods

Preparation of Samples. The preparation procedure and consolidation mechanism of waterglass-based AR coatings is described in detail elsewhere[22]. For the present study, porous films were prepared on slides of soda lime silicate glass (microscope slides, pure white, Marienfeld GmbH, Germany) by dip coating with a diluted 6 wt-% aqueous solution of potassium silicate of a SiO_2/K_2O ratio of 4 (BASF, Germany). The as-coated samples were first dried, then rinsed with deionized water and finally treated at 500°C for 20 min in a muffle furnace. To ensure that the coatings were loaded with water and surfaces were well hydrated[6], samples were kept at least overnight in a desiccator containing a saturated aqueous solution of K_2SO_4 (Analytical grade, Laborchemie Apolda, Germany). Thickness and refractive index of the as-prepared coatings were measured by ellipsometry.

Optical Transmission Measurements. Optical transmission spectra were recorded at room temperature with a standard UV/VIS spectrophotometer (UV-3101PC, Shimadzu, Duisburg, Germany). Optical transmission spectra at higher sample temperature were measured employing a heating stage with the visible spectrophotometer (spectrometer: iDus DV420A, Andor, Belfast, UK; lamp: Xenon lamp XBO150, Osram, Munich, Germany; control unit: Oriel, Newport spectra-physics GmbH, Darmstadt, Germany; heating stage: TS1500, Linkam Scientific Instruments Ltd., Surrey, UK). Transmission spectra in the infrared range were acquired with a FTIR spectrophotometer (IRAffinity, Shimadzu, Duisburg, Germany) at a resolution of 8 cm^{-1} and 512 scans. If not otherwise stated, the optical measurements were conducted under normal laboratory atmospheric conditions (~25°C, 36% r.h.).

Optical Path Length Measurements. The optical path length through the sample (Δn in nm) was determined on a single-side coated slide with a Michelson interference microscope in transmission mode (Jenaval Interphako u.map, Carl Zeiss, Jena, Germany), equipped with a THMS600 heating stage (Linkam Scientific Instruments Ltd., Surrey, UK). In those measurements, the accuracy of optical path length is about 0.5 nm. Optical path length was determined directly, i.e., without further data treatment in two general types of experiments: one was conducted heating the humidity-loaded samples under constant and controlled atmosphere, the other was conducted under isothermal conditions at 30°C, 35°C, 50°C and 70°C, respectively; changing the humidity levels between dry and humid by purging with argon gas or humidified air (~80% r.h. at 24°C). The gas-flow was adjusted to 3 mL/sec, resulting in an exchange (equilibration) time of the heating stage chamber (volume 35 mL) of at least 20 seconds. The time of a single cycle was varied between 180 minutes and 40 minutes.

1. San Vicente, G., Bayón, R., Germán, N. & Morales, A. Long-term durability of sol/gel porous coatings for solar glass covers. *Thin Solid Films* **517**, 3157–3160 (2009).
2. Deubener, J., Helsch, G., Moiseev, A. & Bornhöft, H. Glasses for solar energy conversion systems. *J. Eur. Ceram. Soc.* **29**, 1203–1210 (2009).
3. Vong, M. S. W. & Sermon, P. A. Observing the breathing of silica sol-gel-derived anti-reflection optical coatings. *Thin Solid Films* **293**, 185–195 (1997).
4. Yoldas, B. E. Investigations of porous oxides as an antireflective coating for glass surfaces. *Appl. Opt.* **19**, 1425–1429 (1980).
5. Cathro, K. J., Constable, D. C. & Solaga, T. Durability of porous silica antireflection coatings for solar collector cover plates. *Sol. Energy* **27**, 491–496 (1981).
6. Boissiere, C. *et al*. Porosity and Mechanical Properties of Mesoporous Thin Films Assessed by Environmental Ellipsometric Porosimetry. *Langmuir* **21**, 12362–12371 (2005).
7. Helsch, G., Rädlein, E. & Frischat, G. H. On the origin of the aging process of porous SiO_2 antireflection coatings. *J. Non-Cryst. Solids* **265**, 193–197 (2000).
8. Glaubitt, W. & Löbmann, P. Anti-soiling effect of porous SiO_2 coatings prepared by sol-gel processing. *J. Sol-Gel Sci. Techn.* **59**, 239–244 (2011).
9. Boudot, M., Gaud, V., Louarn, M., Selmane, M. & Grosso, D. Sol-gel based hydrophobic antireflective coatings on organic substrates: a detailed investigation of Ammonia Vapor Treatment (AVT). *Chem. Mater.* **26**, 1822–1833 (2014).
10. Wondraczek, K., Johannsmann, D., Wondraczek, L. & Deubener, J. Application of quartz crystal microbalance for property determination and functionality analysis of thin hydrophilic coatings on glass. *Glass Technol. - Eur. J. Glass Sci. Technol. A* **46**, 179–182 (2005).
11. Zhuravlev, L. T. The surface chemistry of amorphous silica. Zhuravlev model. *Colloid. Surface. A* **173**, 1–38 (2000).
12. Dourdain, S., Britton, D. T., Reichert, H. & Gibaud, A. Determination of the elastic modulus of mesoporous silica thin films by x-ray reflectivity via the capillary condensation of water. *Appl. Phys. Lett.* **93**, 183108 (2008).
13. Ponomarev, Y. N., Petrova, T. M., Solodov, A. M. & Solodov, A. A. IR spectroscopy of water vapor confined in nanoporous silica aerogel. *Opt. Express* **18**, 26062–26067 (2010).
14. Brunet-Bruneau, A., Besson, S., Gacoin, T., Boilot, J. P. & Rivory, J. Reactivity of 3D hexagonal mesoporous silica films to environment studied by infrared ellipsometry. *Thin Solid Films* **447–448**, 51–55 (2004).
15. Asay, D. B. & Kim, S. H. Evolution of the Adsorbed Water Layer Structure on Silicon Oxide at Room Temperature. *J. Phys. Chem. B* **109**, 16760–16763 (2005).
16. Butt, H. J., Graf, K. & Kappl, M. [Liquid Surfaces] *Physics and Chemistry of Interfaces* [5–26] (Wiley-VCH Verlag GmbH & Co., Weinheim, 2006).
17. Ciccotti, M., George, M., Ranieri, V., Wondraczek, L. & Marlière, C. Dynamic condensation of water at crack tips in fused silica glass. *J. Non-Cryst. Solids* **354**, 564–568 (2008).
18. Wondraczek, L. *et al*. Real-Time Observation of a Non-Equilibrium Liquid Condensate Confined at Tensile Crack Tips in Oxide Glasses. *J. Am. Ceram. Soc.* **89**, 746–749 (2006).
19. Gersten, J. I. & Smith, F. W. [Synthesis and Processing of Materials] *The physics and chemistry of materials* [758–762] (John Wiley and Sons Inc., New York, 2001).
20. Dondur, V., Fidler, D., Adnadjević, B. & Rakić, V. The kinetics of water desorption from porous glasses. *J. Therm. Anal.* **32**, 613–622 (1987).
21. Li, X., Li, Z., Xia, Q. & Xi, H. Effects of pore sizes of porous silica gels on desorption activation energy of water vapour. *Appl. Therm. Eng.* **27**, 869–876 (2007).

22. Nielsen, K. H. *et al.* Large area, low cost anti-reflective coating for solar glasses. *Sol. Energ. Mat. Sol. C.* **128**, 283–288 (2014).

Acknowledgments

The authors would like to thank Dr. S. Zankovych (OSIM, FSU Jena) for guidance with the ellipsometric measurements. We further acknowledge financial support by the Thuringian State Ministry of Science and Education through the project NANOSOR.

Author contributions

K.H.N., L.W. and K.W. perceived of the experiments. K.H.N. and L.W. designed model coatings. K.H.N. synthesized the coatings. K.H.N. and T.K. performed the optical analyses. K.H.N., L.W. and K.W. wrote the manuscript. All authors were involved in the discussions and manuscript revisions.

Additional information

Competing financial interests: The authors declare no competing financial interests.

How to cite this article: Nielsen, K.H., Kittel, T., Wondraczek, K. & Wondraczek, L. Optical breathing of nano-porous antireflective coatings through adsorption and desorption of water. *Sci. Rep.* **4**, 6595; DOI:10.1038/srep06595 (2014).